ELECTRONIC SUPPLEMENTARY INFORMATION (ESI)

Distance-Based Paper Analytical Device for Multiplex Quantification of Cytokine Biomarkers Using Carbon Dots Integrated with Molecularly Imprinted Polymer

Kawin Khachornsakkul,[1,2*] Ruben Del-Rio-Ruiz,[1,2] Lita Chheang,[1,2,3] Wenxin Zeng,[1,2] Sameer Sonkusale[1,2*]

[1] *Department of Electrical and Computer Engineering, Tufts University, Medford, MA 02155, USA*

[2] *Nano Lab, Tufts University, Medford, MA 02155, USA*

[3] *Department of Chemistry, Faculty of Science, King Mongkut's University of Technology Thonburi, Bangkok 10140, Thailand*

**To whom correspondence should be addressed. Email: Kawin.khachornsakkul@tufts.edu sameer.sonkusale@tufts.edu*

Table of Contents

Preparation of solution

Phosphate buffer (50.0 mmol L^{-1}, pH 7.4) was prepared by mixing Na_2HPO_4 and NaH_2PO_4 with deionized (DI) water, and then adjusting the pH with NaOH (0.20 mol L^{-1}) and/or HCl (0.20 mol L^{-1}).

Artificial saliva samples were prepared by mixing KH_2PO_4 (2.50 mmol L^{-1}), Na_2HPO_4 (2.40 mmol L^{-1}), $KHCO_3$ (15.0 mmol L^{-1}), NaCl (10.0 mmol L^{-1}), $MgCl_2$ (1.50 mmol L^{-1}), $CaCl_2$ (1.50 mmol L^{-1}) and critic acid (0.15 mmol L^{-1}), subsequently adjusting to pH 6.7 with NaOH (0.20 mol L^{-1}) and/or HCl (0.20 mol L^{-1}).[7]

Artificial sweat samples were prepared in accordance with prior literature. Concisely, urea (0.10 w/v%), NaCl (0.50 w/v%), and lactic acid (0.10 w/v%) are mixed and adjusted to pH 6.5 with NaOH (0.20 mol L^{-1}) and/or HCl (0.20 mol L^{-1}).[39]

Design and fabrication of the UV-light black box

The UV-light black chamber was designed using computer aided Solidworks (Dassault Systems, SolidWorks Corporation, Waltham, MA). It consisted of six black acrylic sheets (one base, four side-walls and one removable top) to form an opaque chamber, as shown in **Fig. S1a**. 6.35mm-thick acrylic sheets were designed with crenels-like shapes on their edges, to accurately align and easily assemble the chamber. The total dimensions of the chamber were 121.0 mm, 121.0 mm, and 121.0 mm (width x length x height), as shown in **Fig. S1b**. Black acrylic sheets (B09DCM1W4H) were laser-cut using a 70W BossLaser LS1416 to obtain the base, 4 side-walls and the removable top for each chamber. Black hot glue (B08FB3J8HM) was applied, using a commercially available hot glue gun (T-TOVIA), on the crenels, prior to the assembly, to increase the chamber's overall robustness. A total of four 24.5 W-UV light-emitting diodes (LEDs) (B09F69T3H9) with a narrow spectral output centered at 400.0 nm ± 5.0 nm, and a color rendering index of 90. They were attached to the top side of the chamber, controlled by high quality polyamide (Nylon PA66) single pole, single throw (SPST) switch (B07Y1GDRQG), and powered by an external 12V power supply. The removable top was designed with 3 holes. A 40 mm-diameter hole, in the center, to acquire images using a mobile phone. A rectangle hole, positioned in a corner of the removable top (**Fig. S1b**), to insert the secure the switch that controls the UV light LEDs. Finally, a 5 mm-diameter hole was insert on its side, to insert the cable for power-supplying the UV light LEDs.

Surface characterization of the developed dPADs

We characterized the surface of modified structures of the detection zone of the dPADs using a SEM image and EDS analysis. **Fig. S5(a)** displayed the structure of bare paper, where the cellulose fibers forming a non-uniform three-dimensional network can be observed. we observed a reduction in the size of pores, resulting in a smoother surface (**Fig. S5(b)**). Remarkably, the EDS analysis demonstrated that there were increase in the percentage of carbon (C) and oxygen (O) atoms after CMC modification owing to their structure of carboxylic cellulose, confirming the CMC-modified paper substrate. While the morphological changes in the paper surface were not visually apparent after coating with CDs (**Fig. S5(c)**). However, EDS analysis revealed the presence of nitrogen atoms (N) associated with an amino group of the CDs particles, indicating the successful grafting of the CDs onto the surface of paper fibers (**Fig. S5(d)**). The fabrication of this fluorescent paper somehow relies on an amidation reaction between the carboxylic group of the CMC-modified paper and the amino group of the synthesized CDs.[28,41] Moreover, the surface of the paper had obvious blue fluorescence, resulting in the successful grafting the CDs particles into the paper fiber. In our experiment, we observed numerous slight agglomerates on the surface of the paper fiber (**Fig. S6(a-c)**), suggesting that there were imprinted shell layers on the paper substrate.[28] However, upon removing the template, the surface become more smoother like paper modified with CMC-CDs (**Fig. S6(d-f)**). This result indicates notable differences in the paper's surface between the stages of binding and removing the MIP layer on the paper membrane.

To further confirm the integration of MIP onto the paper sensor, we examined the functional groups on the CMC-CDs modified paper without and with the MIP layer. In **Fig. S7(a)**, the FT-IR spectrum of the CMC-CDs modified paper indicated absorption bands at 3434, 2924, 1110, and 1058 cm^{-1} corresponding to stretching vibrations of O-H, C-H, and C-O-C,

characteristic of cellulose paper.[42] Additionally, strong absorption bands at 1620 cm^{-1} for COO- and 1423 cm^{-1} for carboxyl groups (as salts) were observed, demonstrating the achievable immobilization of CMC onto the paper membrane.[43] Peaks at 1586, and 1078 cm^{-1} were also identified, corresponding to C=C, and C-O-C stretching vibrations, respectively. Furthermore, a peak at 1720 cm^{-1} was observed for the asymmetric stretching of C=O groups. Bending vibrations of C-N and C=N were also detected, signifying the characteristic features of the CDs.[38,41] In **Fig. S7(b)**, the absorption spectrum of CMC-CDs modified paper with the MIP layer exhibited prominent peaks at 3312, 1609, and 1497 cm^{-1}, corresponding to N-H stretching, a superposition of N-H bending and phenolic C=C stretching, and aromatic C=H bending vibration, respectively. These functional groups, indicative of catechol and amine groups, confirm the formation of a PDA layer on the paper substrate.[30] Consequently, the surface modification of the MIP layer onto the paper substrate in this developed approach is successful.

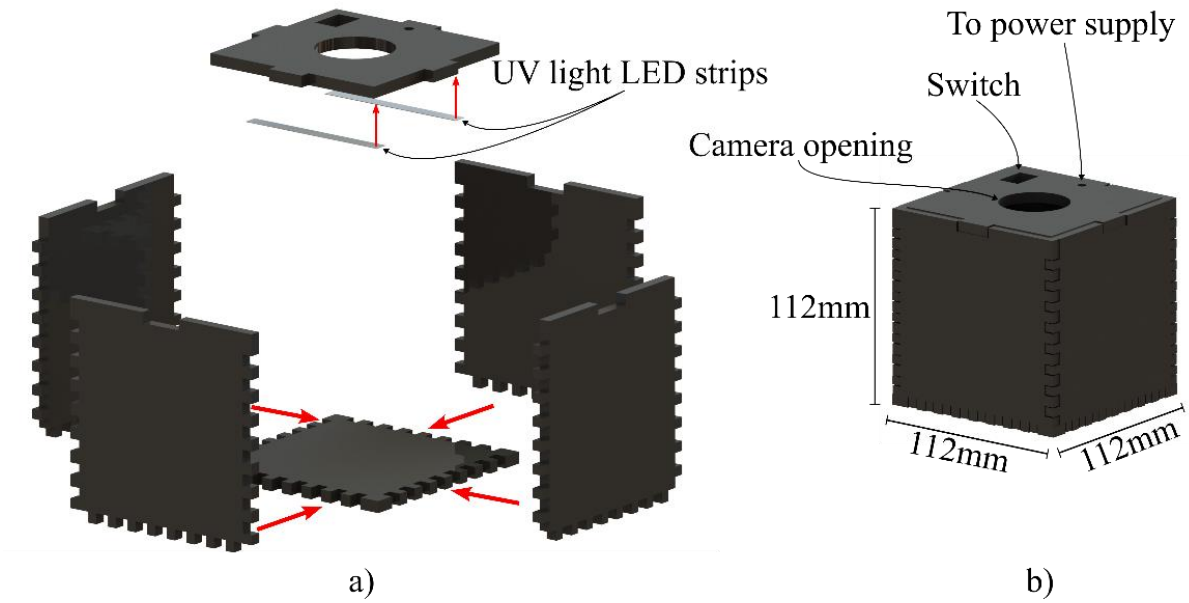

Fig. S1 3D Design and assembly of the UV light black chamber (a) individual parts and assembly process and (b) assembled black chamber illustrating its overall dimensions and functionalities.

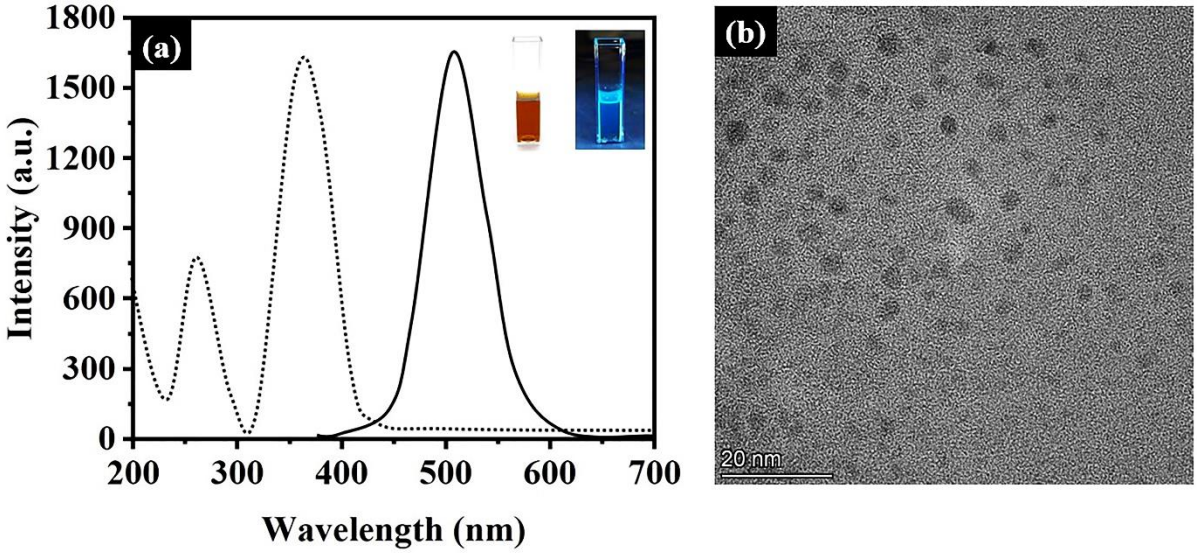

Fig. S2 Characterization of the synthesized CDs in this work using (a) fluorescence spectrophotometer with their characteristic colors (inserted image) and (b) their TEM image.

We characterized the formation of the synthesized CDs using a fluorescence spectrophotometer as shown in **Fig. S2(a)**. The maximum excitation and emission wavelength were found at 365 (dot line) and 520 nm (solid line), respectively. The color of the CDs solution was dark yellow under ambient light, but it emitted blue fluorescence under UV-light. We further investigated their particles sizes using TEM. The measurement demonstrated the size of the synthesized CDs was 4.0 ± 1.0 nm as shown in **Fig. S2(b)**. These above characterizations could confirm the CDs in the proposed method.

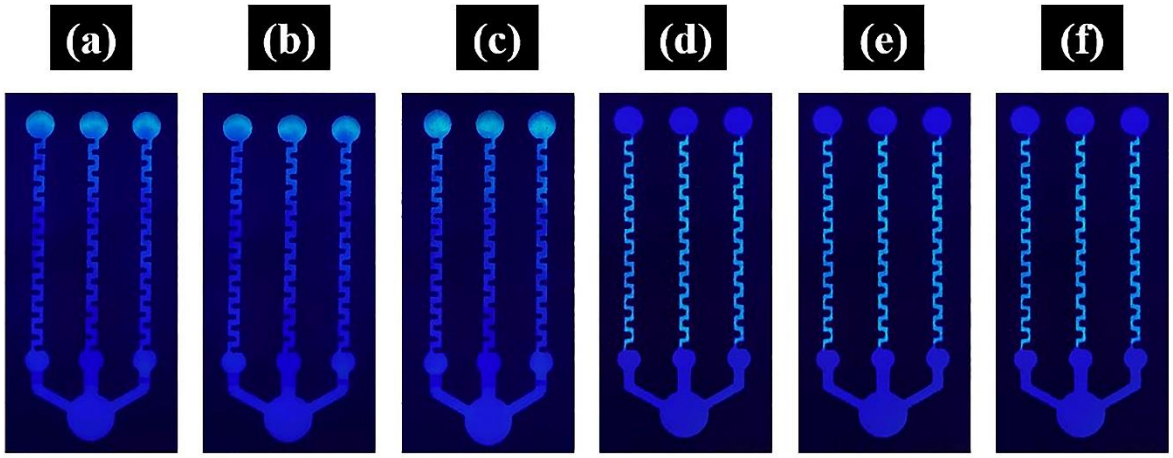

Fig. S3 Image of the developed dPADs at different concentration of CMC including (a) 0.25, (b), 0.50, (c) 1.0, (d) 2.0, (e) 3.0, and (f) 4.0. mg mL^{-1}.

We evaluated the CMC concentration immobilized into the detection zones of the dPADs ranging from 0.25 to 4.0 mg mL^{-1} by adding 60.0 µL of PBS solution in the sample zone. In **Fig. S3**, we noted that there were no significant fluorescence emissions in the detection zones when the CMC concentration was below 2.0 mg/mL. Instead, fluorescence emissions were observed in the waste zones, suggesting that CDs couldn't interact with CMC through the amidation reaction and thus were not absorbed in the detection zones. However, the fluorescence emission in the detection zones were initially obtained when the concentration of CMC was larger than 2.0 mg mL^{-1}. However, fluorescence emissions in the detection zones became apparent when the CMC concentration exceeded 2.0 mg mL^{-1}. This indicated successful immobilization in this zone and could not flow although solution was introduced. As a result, we opted for a CMC concentration of 2.0 mg mL^{-1} in our experiments in order to reduce the reagent consumption.

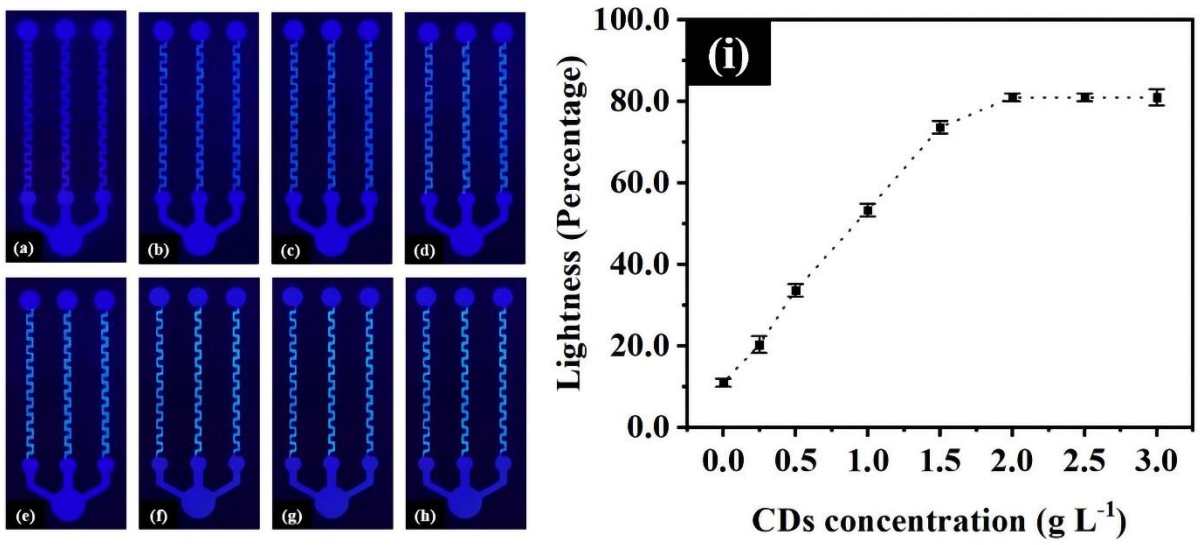

Fig. S4 Image of the developed dPADs at different concentration of CDs including (a) 0.0, (b), 0.25, (c) 0.50, (d) 1.0, (e) 1.50, (f) 2.0, (g) 2.50, and (g) 3.0 g L^{-1} (n=3), and (i) the relationship of the lightness signals and CDs concentration on paper substrate (n = 3).

In this experimental study, we assessed the concentration of CDs immobilized in the detection zones by measuring the brightness of their blue fluorescence. We conducted this measurement using the lightness channel (unit; percentage) within the Hue-Saturation-Lightness mode of the Color Grab application (Loomatix, version 3.6.1) on a smartphone application.[40] **Fig. S4** visually demonstrates that the blue fluorescence emission in the detection zones grew brighter with increasing CD concentrations, which results were similar to the detection of the lightness intensity (**Fig. S4(i)**). Notably, the intensity plateaued when concentration of the CDs was beyond 2.0 g L^{-1}. Consequently, we selected this CD concentration as it was sufficient for our method.

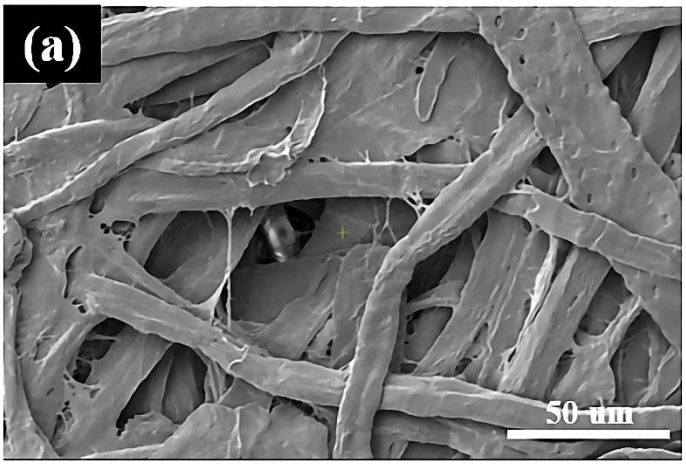

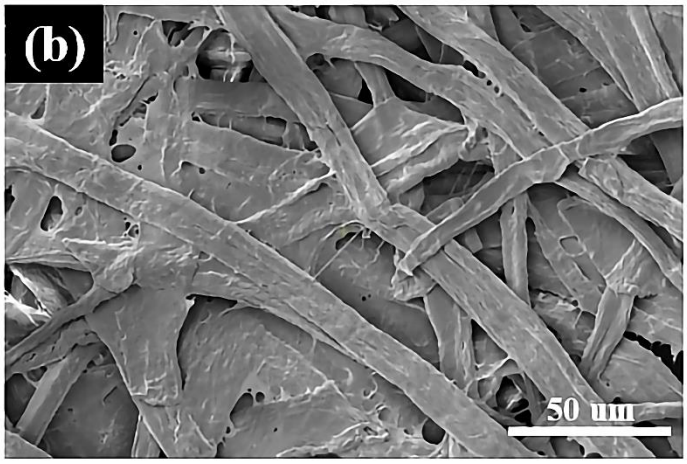

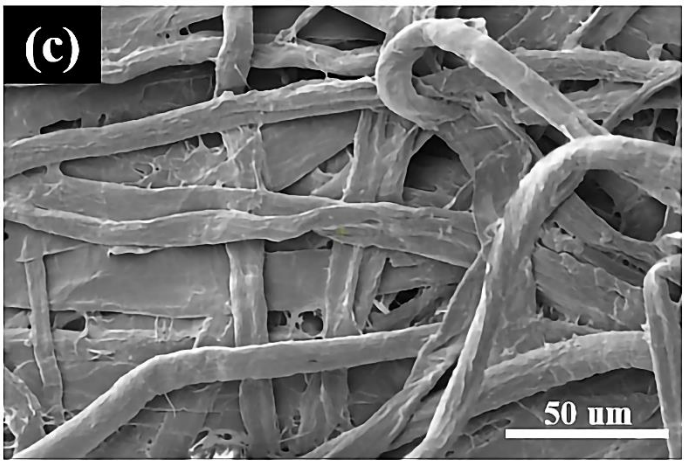

(d) EDS analysis

a	b	c
C 42.8 % O 51.6 %	C 52.7 % O 57.4 %	C 51.5 % O 56.9 % N 5.4 %

Fig. S5 SEM images of (a) bare paper, (b) CMC modified paper, (c) CMC modified paper coated with CDs (c), and (d) their EDS analysis. Note SEM image with magnification of 2000x.

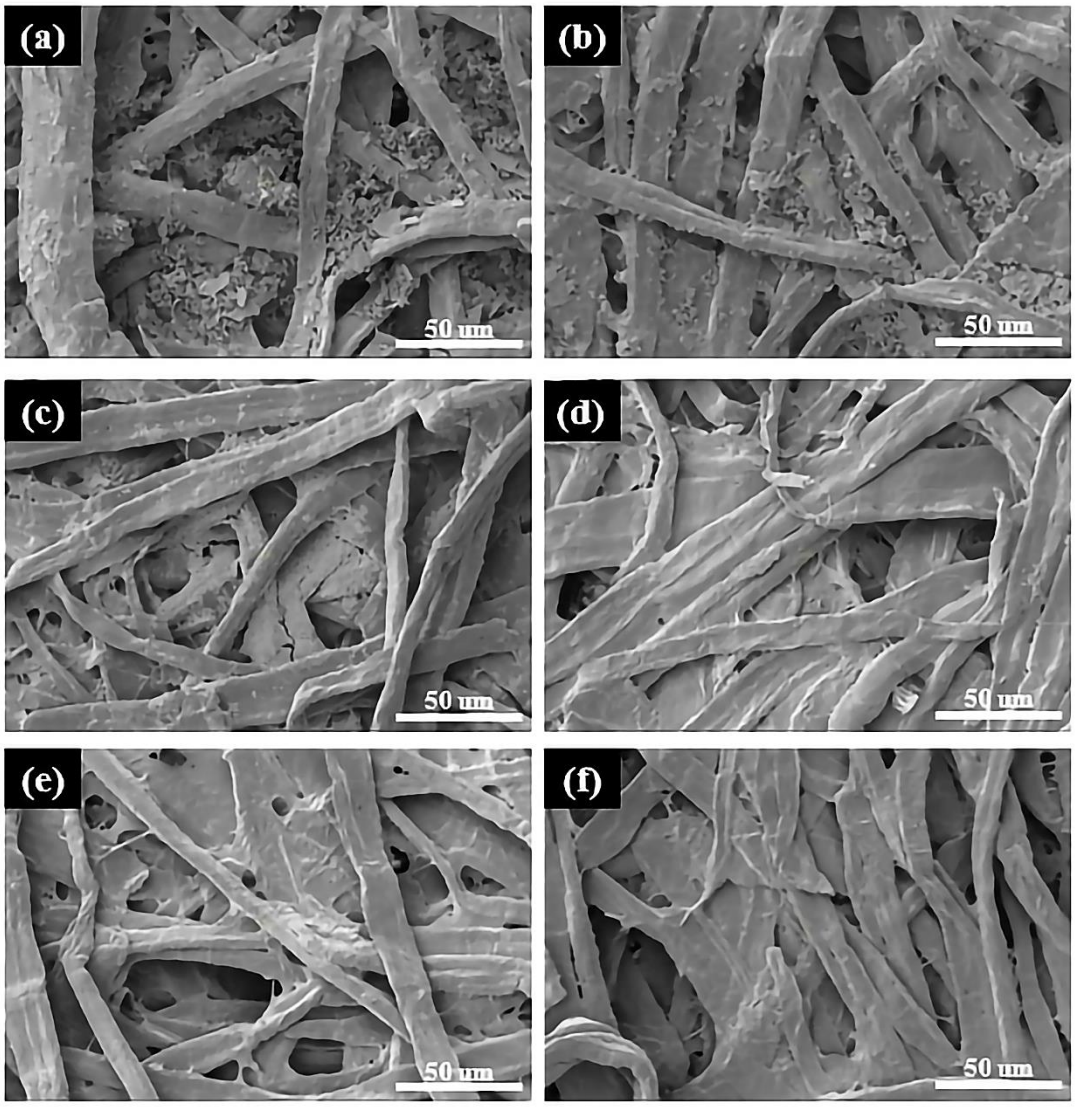

Fig. S6 SEM image of CMC modified paper coated with CDs@MIPs before template removal step for (a) CRP, (b) TNF-α, (c) and IL-6, and after template removal step for (d) CRP, (e) TNF-α, (f) and IL-6. Note SEM image with magnification of 2000x.

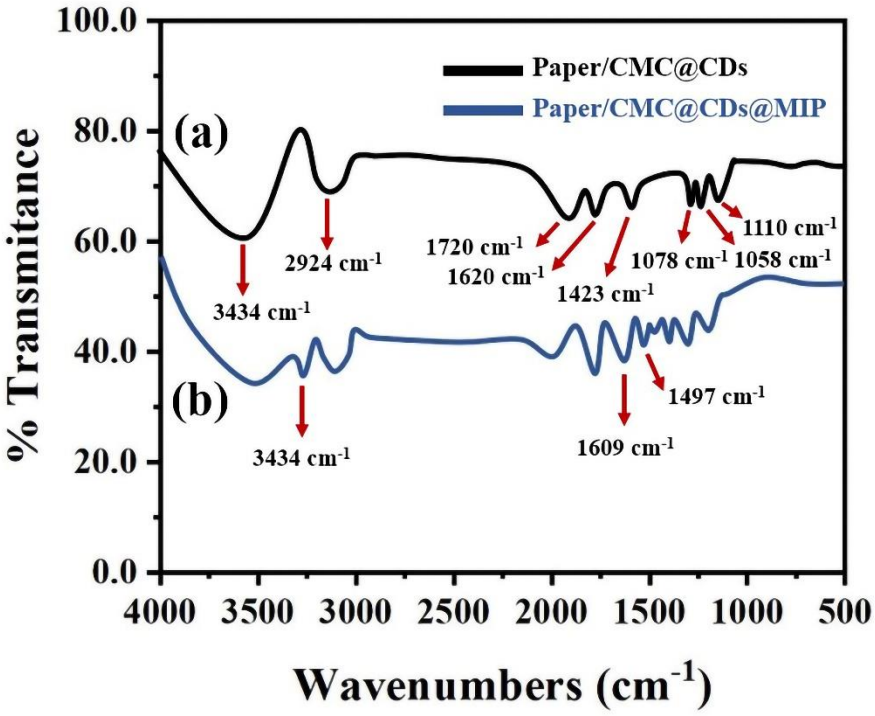

Fig. S7 FT-IR spectrum of CMC@CDs modified paper membrane without (a) and with (b) MIP layer.

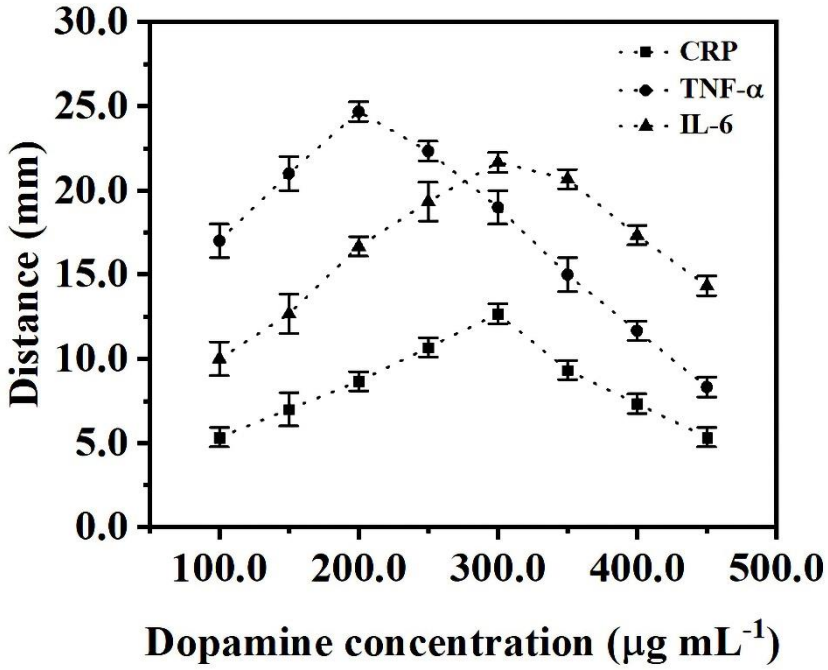

Fig. S8 Demonstrate the distance signals of dopamine concentration for (■) CRP (12.0 pg mL^{-1}), (●) TNF-α (2.0 pg mL^{-1}), and (▲) IL-6 (10.0 pg mL^{-1}) detection in the developed dPADs (n = 3).

Dopamine concentration was optimized due to its impact on the formation of the MIP on the developed dPAD sensor. We evaluated its concentration ranging from 100.0 to 450.0 μg mL^{-1} as indicated in **Fig. S8**. The distance signals notably increased until reaching 300.0 μg mL^{-1} for CRP and IL-6, and 200.0 μg mL^{-1} for TNF-α, respectively. Beyond these thresholds, there was a distinct decline in distance signals. Because higher dopamine concentration leads to an increase in the polymer film thickness and subsequent embedding of the template within the polymer layer, which is difficult to remove for the cavities,[31] resulting in the lower capacity to bind analyte to the imprinted polymer in the microchannel. Similarly, at lower concentrations, the thin layer of polymer membrane is insufficient for the formation of specific cavities and binding sites.[25] So, the dopamine concentrations at 300.0 μg mL^{-1} for CRP and IL-6 and 200.0 μg mL^{-1} for TNF-α were chosen as a suitable level in our sensor.

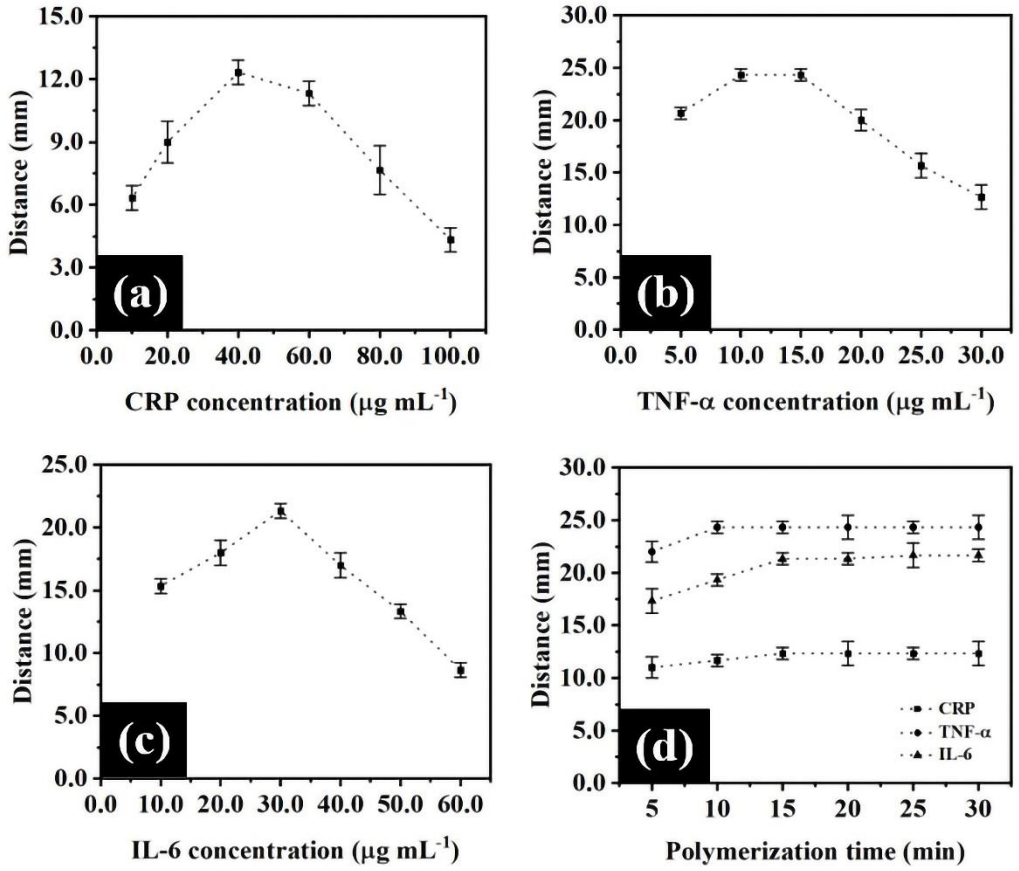

Fig. S9 Demonstrate the distance signals of template concentrations of (a) CRP, (b) TNF-α, (c) IL-6, and (d) polymerization time for (■) CRP (12.0 pg mL^{-1}), (●) TNF-α (2.0 pg mL^{-1}), and (▲) IL-6 (10.0 pg mL^{-1}) detection in the developed dPADs (n = 3).

Following that, the template concentrations were optimized since they can affect the number and complementary shape of the imprinted cavities on the paper substrate. We observed that there were dramatic increases in the distance signals as template concentrations for all analytes as indicated in **Fig. S9(a-c)**. Nonetheless, the distance signals promptly decreased when their concentrations were 40.0, 10.0, and 30.0 μg mL^{-1} for CRP, TNF-α, and IL-6 monitoring, respectively. Since a larger number of template molecules can be embedded into the MIP surface, resulting in the hard removal of the template after an imprinting procedure.[26] Accordingly, it

reduces the rebinding performance between analyte and cavity sites in the developed sensor. So, we opted for template concentrations at 40.0, 10.0, and 30.0 μg mL^{-1} for CRP, TNF-α, and IL-6, respectively, to achieve the highest sensitivity in our technique. Next, the influence of the polymerization time on the MIP formation is investigated since it is factor tied to binding efficiency. We thus varied the polymerization time for the MIP formation within the range of 5.0 to 30.0 min. In **Fig. S9(d)**, the results demonstrated the obvious increment in the distance signals as proportional to the time. Notably, the distance signals were immediately stable when the time was higher than 15 min for CRP and IL-6 and 10 min for TNF-α. Hence, we selected these polymerization times as an optimum value to reduce the time consumption of the assay procedure.

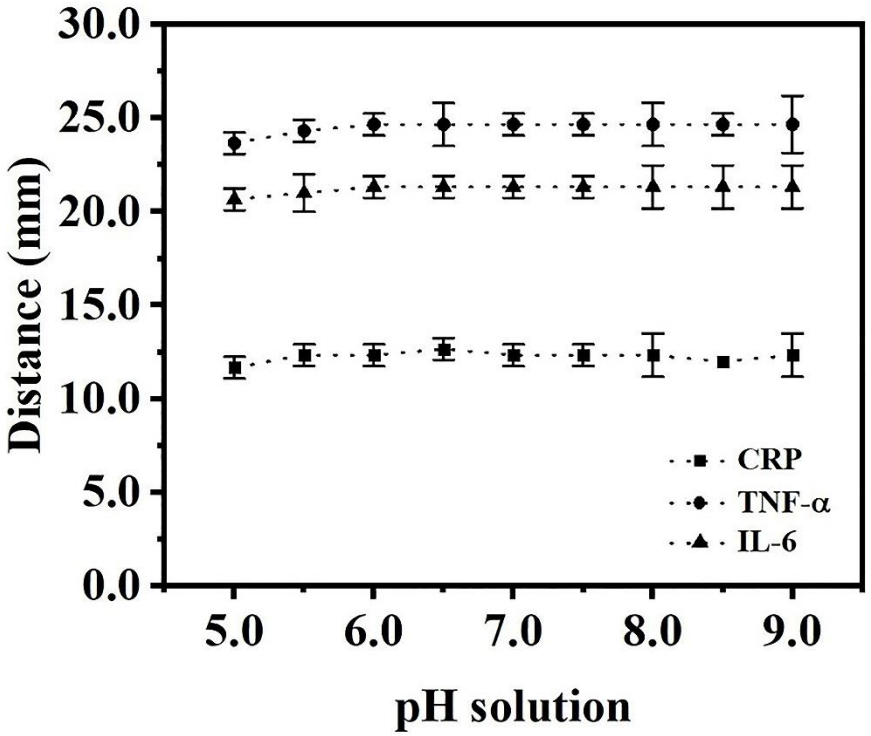

Fig. S10 Demonstrate the distance signals of pH solution for (■) CRP (12.0 pg mL^{-1}), (●) TNF-α (2.0 pg mL^{-1}), and (▲) IL-6 (10.0 pg mL^{-1}) detection in the developed dPADs (n = 3).

We also tested whether the impact on pH buffer can affect the binding of the analyte with the MIP on paper substrate, we changed the pH of PBS ranging from 5.0 to 9.0 into the pretreatment zone of the sensor, as shown in **Fig. S10**. Interestingly, we found that the distance values for all biomarker detections remained remarkably consistent towards all pH values, rendering the extensive application in broad pH conditions compared to previous methods. We altogether conducted a pH of 7.5 for our experiment as it is compatible with the human sample condition.

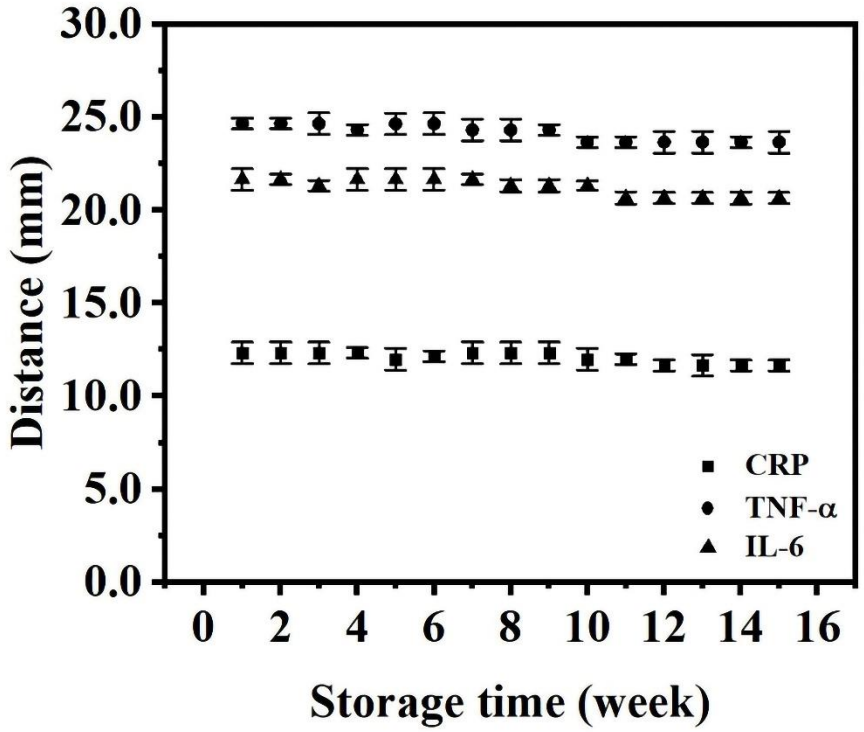

Fig. S11 Demonstrate the distance signals of storage time for (■) CRP (12.0 pg mL^{-1}), (●) TNF-α (2.0 pg mL^{-1}), and (▲) IL-6 (10.0 pg mL^{-1}) detection in the developed dPADs (n = 3).

Besides, the long-term stability of the proposed sensor was investigated by detecting the distance signals over a period of 15 weeks with the device stored in a seal bag at 4 ± 1 °C. In **Fig. S11** showed that the distance signals for CRP, TNF-α, and IL-6 detection did not deviate over 5.0% from the initial week, resulting in the remarkable stability for practical application.

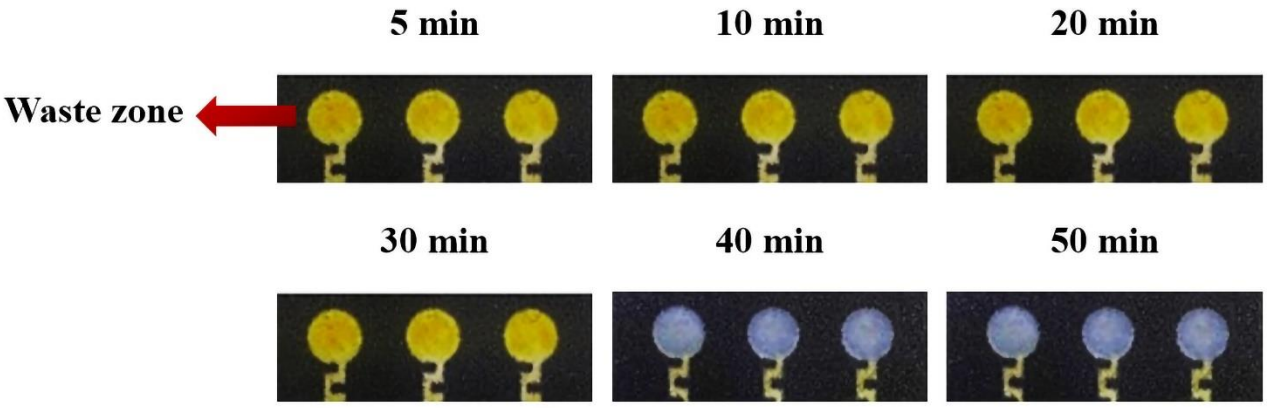

Fig. S12 Image of the waste zone of the developed dPADs. For experiment, 3.0 µL of 0.50 mg mL^{-1} bromophenol blue (BPB) were deposited on waste zone and left to dry at room temperature.[7,19]

To run the experiment, 60.0 µL of BSA solution at 2.0 mg mL^{-1} was introduced into the sample zone of the developed dPAD, and the color in the waste zone was observed as a time.

To prove whether this reaction will influence final measurement due to the solvent evaporation, we observed some change in color due to the reaction between bovine serum albumin (BSA) and bromophenol blue (BPB) in the waste zone.[7,19] We added BSA solution at 2.0 mg/mL into the sample zone. **Fig. S12** indicated that the blue color of BSA-BPB complex initially appeared when the reaction time reached 40 min. This result demonstrates no significant influence on the solution evaporation in our method.

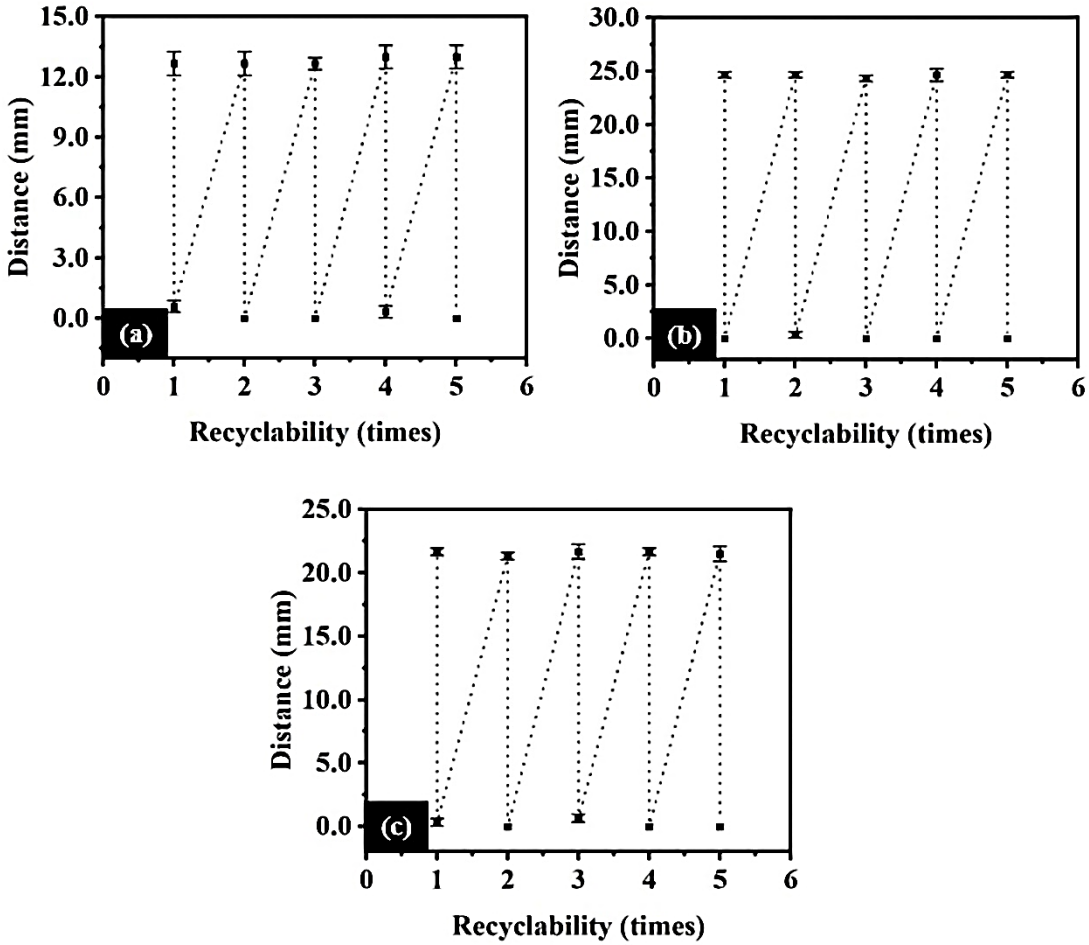

Fig. S13 Demonstrate the distance signal for reusability of the developed dPAD sensor for detection of (a) CRP at 12.0 pg mL^{-1}, (b) TNF-α at 2.0 pg mL^{-1}, and (c) IL-6 at 10.0 pg mL^{-1} in the proposed method (n = 3).

The recyclability of the device was assessed by evaluating distance signals through a series of template removal and rebinding procedures. The distance signals were initially reduced to 0.0 mm upon template removal. Subsequently, they increased to 12.33 mm, 24.33 mm, and 21.66 mm for CRP, TNF-α, and IL-6, respectively, after rebinding the template (**Fig. S13**). These cycles were repeated five times, consistently yielding results without significant differences from the first to the fifth cycle. However, beyond the fifth cycle, we observed deterioration in the paper substrate. Therefore, we conclude that the recyclability of our dPAD is at least five times.

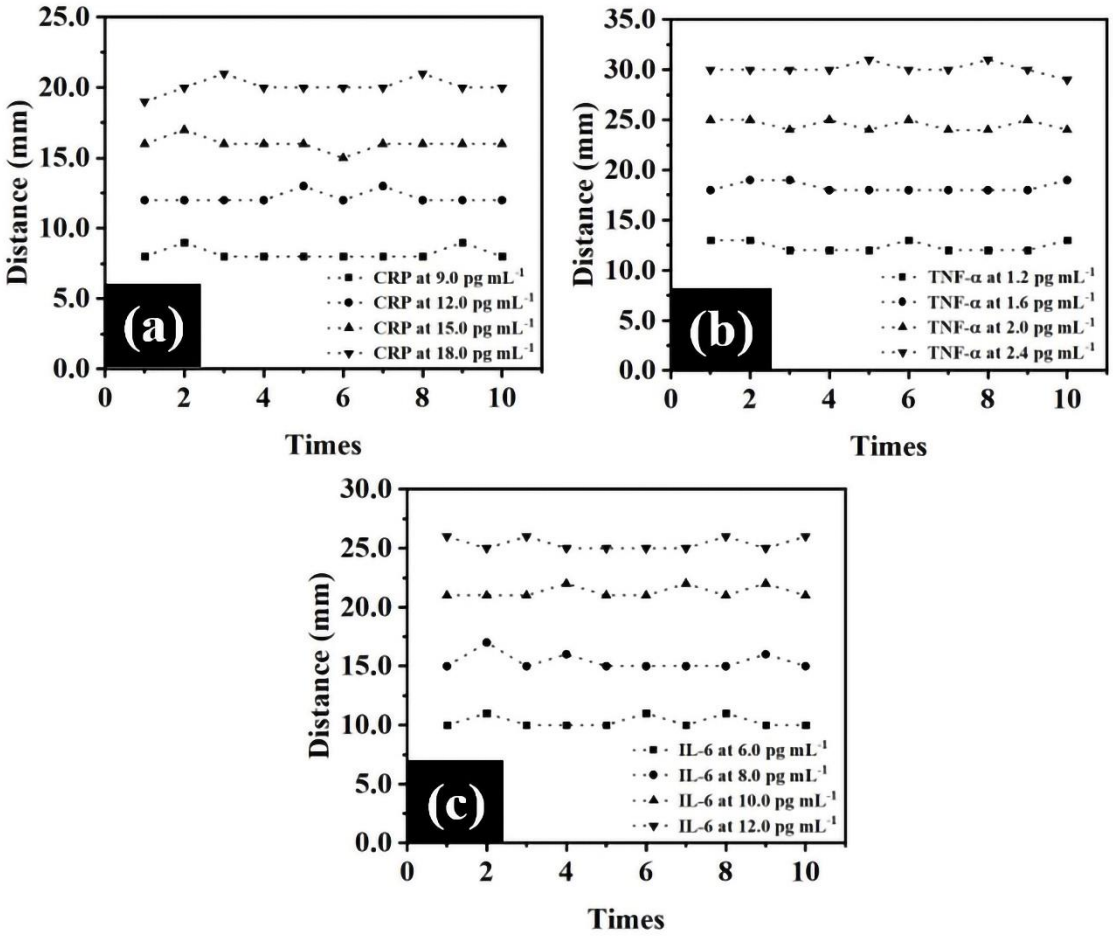

Fig. S14 Demonstrate the distance signals for reproducibility of the developed dPADs including (a) CRP at (■) 9.0, (●) 12.0, (▲) 15.0, and (▼) 18.0 pg/mL, (b) TNF-α at (■) 1.2, (●) 1.6, (▲) 2.0, and (▼) 2.4 pg/mL, and (c) IL-6 at (■) 6.0, (●) 8.0, (▲) 10.0, and (▼) 12.0 pg mL^{-1} in the proposed method.

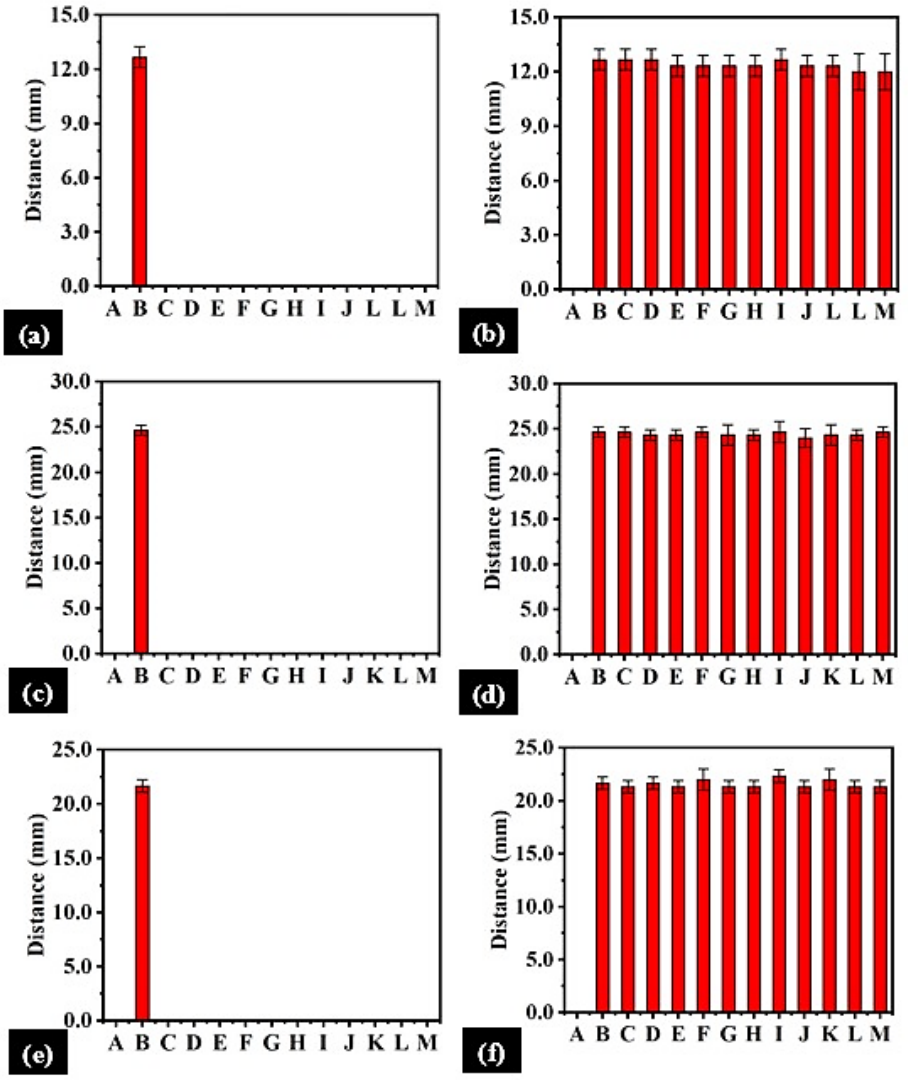

Fig. S15 Demonstrate the distance signals of the selectivity studies of (a) CRP, (c) TNF-α, and (e) IL-6; (A) a blank solution, (B) CRP (12.0 pg mL^{-1}), TNF-α (2.0 pg mL^{-1}), or IL-6 (10.0 pg mL^{-1}), and solutions of a range of potentially interfering substances including (C) bovine serum albumin (100.0 g L^{-1}), (D) CRP (10.0 mg mL^{-1}) for TNF-α and IL-6 detection, TNF-α (20.0 pg mL^{-1}) for CRP and IL-6 detection, and IL-6 (10.0 pg mL^{-1}) for CRP and TNF-α detection, (E) creatinine (1.0 mg mL^{-1}), (F) cortisol (50.0 ng mL^{-1}), (G) dopamine (50.0 pg mL^{-1}), (H) fructose (10.0 mmol L^{-1}), (I) glucose (10.0 mmol L^{-1}), (J) IL-6 (10.0 pg mL^{-1}), (K) lactic acid (50.0 μmol L^{-1}), (L) urea (50.0 mmol L^{-1}), and (M) uric acid (50.0 μmol L^{-1}). In (b), (d), and (f) distance signals measured

for (A) a blank, (B) CRP (12.0 pg mL^{-1}), TNF-α (2.0 pg mL^{-1}), or IL-6 (10.0 pg mL^{-1}), and (C-M) mixtures of CRP (12.0 pg mL^{-1}), TNF-α (2.0 pg mL^{-1}), or IL-6 (10.0 pg mL^{-1}) and above concentrations of the potentially interfering substances (n = 3).

Selectivity and Interferent Effects

The selectivity of the developed method was examined by measuring the distance signals in the presence of various potential interferent substrates that could be present in human biological samples. Experimentally, we detected analytes, CRP (12.0 pg mL^{-1}), TNF-α (2.0 pg mL^{-1}), and IL-6 (10.0 pg mL^{-1}), and potential interferences at concentration given by a clinical laboratory. In **Fig. S14 (a, c, and e)** revealed that the apparent distance signals were acquired from only target analytes, while the distance signals of the other substrates were 0.0 mm equal to the blank signal. Additionally, we tested the interferent effects by measuring the distance signal of mixture solution between target biomolecule and interferent agents. **In Fig. S14 (b, d, and f)** indicated that the distance signals obtained from the mixture solution differed by no more than 5.0% from those obtained without the interferent substrates. Our developed method thus exhibits remarkable selectivity, showing no significant interferent effects for simultaneous detection of these cytokine biomarkers. Importantly, this selectivity is achieved without the need for expensive reagents such as antibodies and enzymes.

The calculation of dissociation constant (K_d)

In this work, the binding affinity was studied in term of the equilibrium dissociation constant (K_d) for evaluating the intermolecular interaction strengths between the MIP cavity and the target proteins.

Assuming that a MIP cavity was bound with target analyte's molecule, the K_d can be calculated through the equation below;

$$K_d = [MIP]\,[Analyte] / [MIP\text{-}analyte]$$

where [MIP], [Analyte], and [MIP-analyte] are the concentration of unbound MIP, unbound analytes and bound MIP-analyte in the detection zone of the dPADs, respectively. The distance signals with a half of maximum signal demonstrated that the bound MIP-analyte were equal to the concentration of unbound MIP ([MIP] = [MIP-analyte]). Hence, the K_d is equal to analyte concentration.[29]

Based on the working linear range of the developed device in **Fig. 3**, the linear regression equation is Y = 1.2833X – 2.7926 for CRP detection, Y= 13.318X – 2.5484 for TNF-α detection and Y = 2.3759X – 2.8105 for IL-6 detection, where Y is distance signals and X is analyte concentration. We found the average maximum distance signals (Y_{max}) are 28.67, 39.33, and 35.00 mm for CRP, TNF-α, and IL-6, respectively. So, the half values of Y_{max} ($Y_{max/2}$) are 14.34, 19.67, and 17.5 mm for CRP, TNF-α, and IL-6, respectively. Finally, the K_d values are calculated as 13.35, 1.67, and 8.55 pg mL^{-1} for CRP, TNF-α, and IL-6, respectively.

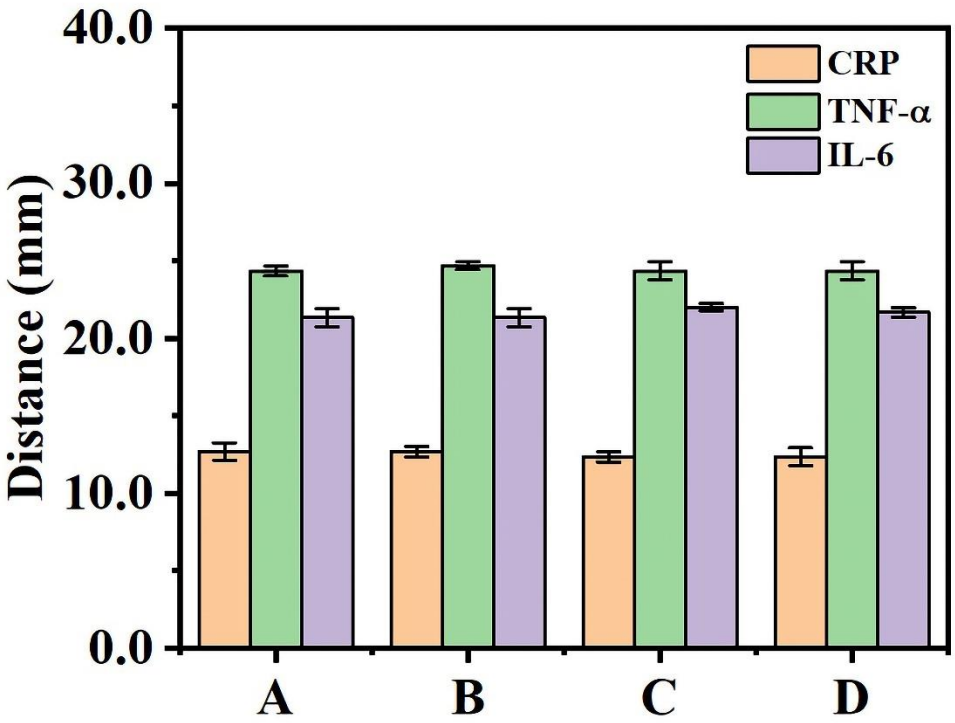

Fig. S16 Demonstrate the distance signals of CRP at 12.0 pg mL^{-1} (orange bar), TNF-α at 2.0 pg mL^{-1} (green bar), and IL-6 at 10.0 pg mL^{-1} (purple bar) detection in the various sample matrices, including (A) human serum, (B) human urine, (C) artificial saliva, and (D) artificial sweat (n = 3).

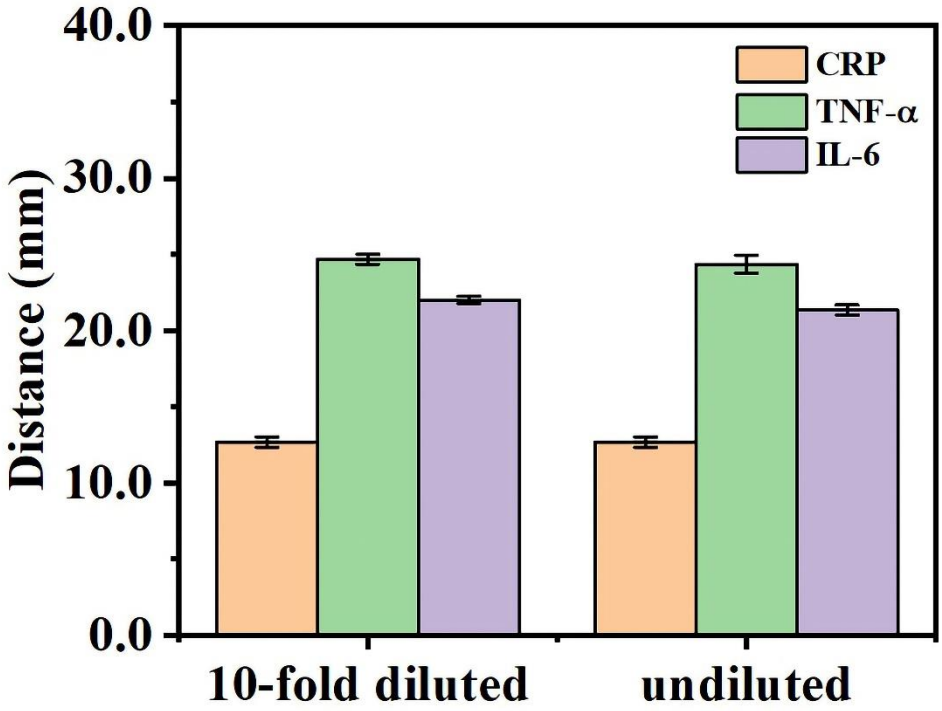

Fig. S17 Demonstrate the distance signals of CRP at 12.0 pg mL^{-1} (orange bar), TNF-α at 2.0 pg mL^{-1} (green bar), and IL-6 at 10.0 pg mL^{-1} (purple bar) detection in the human control serum with 10-fold dilution and undilution (n = 3)

Table S1 Result of CRP level in the certificate reference human serum samples analysis by our developed method (n = 3).

Total found (mg L^{-1})	**Specific label (mg L^{-1})**	**T-test**	**%RSD**
41.0 ± 0.5	41.2	0.53	1.21